Mon. Not. R. Astron. Soc. **392,** 91–103 (2009) doi:10.1111/j.1365-2966.2008.14063.x

Low-luminosity gamma-ray bursts as a distinct GRB population: a firmer case from multiple criteria constraints

Francisco J. Virgili,[1⋆] En-Wei Liang[2⋆] and Bing Zhang[1⋆]

[1] *Department of Physics and Astronomy, University of Nevada Las Vegas, Las Vegas, NV 89154, USA*
[2] *Department of Physics, Guangxi University, Nanning 530004, China*

Accepted 2008 October 9. Received 2008 September 30; in original form 2008 January 30

ABSTRACT

The intriguing observations of the *Swift*/Burst Alert Telescope (BAT) X-ray flash (XRF) 060218 and the BATSE-*BeppoSAX* gamma-ray burst GRB 980425, both with much lower luminosity and redshift compared to other observed bursts, naturally lead to the question of how these low-luminosity (LL) bursts are related to high-luminosity (HL) bursts. Incorporating the constraints from both the flux-limited samples observed with *Compton Gamma-ray Observatory (CGRO)*/BATSE and *Swift*/BAT and the redshift-known gamma-ray burst (GRB) sample, we investigate the luminosity function for both LL and HL GRBs through simulations. Our multiple criteria, including the $\log N - \log P$ distributions from the flux-limited GRB sample, the redshift and luminosity distributions of the redshift-known sample and the detection ratio of HL and LL GRBs with *Swift*/BAT, provide a set of stringent constraints to the luminosity function. Assuming that the GRB rate follows the star formation rate (SFR), our simulations show that a simple power law (PL) or a broken power-law model of luminosity function fails to reproduce the observations and a new component is required. This component can be modelled with a broken power, which is characterized by a sharp increase in the burst number at around $L < 10^{47}$ erg s^{-1}. The lack of detection of moderate-luminosity GRBs at redshift $\sim$0.3 indicates that this feature is not due to the observational biases. The inferred local rate, ρ_0, of LL GRBs from our model is $\sim$200 Gpc^{-3} yr^{-1} at $\sim 10^{47}$ erg s^{-1}, much larger than that of HL GRBs. These results imply that LL GRBs could be a separate GRB population from HL GRBs. The recent discovery of a local X-ray transient 080109/SN 2008D would strengthen our conclusion if the observed non-thermal emission has a similar origin as the prompt emission of most GRBs and XRFs.

Key words: gamma-rays: bursts – gamma-ray: observations – methods: statistical.

1 INTRODUCTION

Long-duration gamma-ray bursts (GRBs) are believed to be tied to the death of massive stars (Colgate 1974; Woosley 1993; Hjorth et al. 2003; Stanek et al. 2003; Campana et al. 2006). Of the roughly 6000 bursts observed since the late 1960s (see e.g. http://heasarc.gsfc.nasa.gov/grbcat/), almost 100 have redshift measurements. Observations show that long GRBs are scattered over a large redshift and luminosity[1] range, from $z = 0.0085$ to 6.7[2] (see Table 3) and $L = 10^{46}$–10^{54} erg s^{-1}. Most of these bursts have high luminosity (HL; $L >$ several 10^{48} erg s^{-1}) with the exception of two peculiar bursts, GRBs 980425 and 060218, which have extremely low redshift and luminosity measurements $(z, L) = (0.0085, 4.7 \times 10^{46}\,\mathrm{erg\,s^{-1}})$ and $(0.033, 6.03 \times 10^{46}\,\mathrm{erg\,s^{-1}})$, respectively (Tinney et al. 1998; Mirabal et al. 2006). It remains unclear whether the low-luminosity (LL) GRBs are due to unusual progenitor properties or a unique population with an intrinsic difference in the central engine, i.e. black hole versus magnetar (Mazzali et al. 2006; Soderberg et al. 2006; Toma et al. 2007).

One empirical way to look into this problem is to see whether observational data collected so far are still consistent with LL GRBs

⋆E-mail: virgilif@physics.unlv.edu (FJV); lew@physics.unlv.edu (EWL); bzhang@physics.unlv.edu (BZ)

[1] Throughout the text, the burst luminosity refers to the isotropic equivalent value, which does not include the possible correction of the unknown beaming factor of the GRBs.

[2] This record redshift measurement is from GRB 080913. It remains unclear what category this particular burst belongs to, type I or type II, and is not included in the statistical analysis of this work.

as a natural extension of HL GRBs to low luminosities in a continuous luminosity function (LF), or if LL GRBs form a distinct new LF component. We have suggested that the latter possibility (two-component LF model) is necessary based on the redshift-known sample of GRBs after the discovery of GRB 060218 (Liang et al. 2007). Such a possibility has also been considered as a hypothesis in the *BeppoSAX* era (Coward 2005). On the other hand, although Guetta & Della Valle (2007) (hereafter G07) agreed that the two-component model is possible, they also argued that the z-known GRB sample may also be consistent with a single-component model with a steeper slope in the LF so that more LL GRBs are accounted for.

Comparing observational data with simulations is a useful way to address the relationship between LL GRBs and HL GRBs. It is an important task to constrain the LF, $\Phi(L)$, and local rate of GRBs, ρ_0, in a manner that can self-consistently reproduce various observations. In particular, the current LL-GRB population studies have been focused on the z-known sample only. They were not confronted with the existing $\log N - \log P$ distribution of the BATSE GRB sample. The $\log N - \log P$ distribution (or $V/V_{\max}$ distribution) addresses the statistical properties of GRBs regardless of their redshift, and carries essential information of the GRB LF. For HL GRBs, this criterion has been utilized extensively (e.g. Schmidt 2001; Lloyd-Ronning, Fryer & Ramirez-Ruiz 2002; Norris 2002; Stern, Atteia & Hurley 2002; Guetta, Piran & Waxman 2005, hereafter G05) and was confronted with simulations (Lloyd-Ronning, Dai & Zhang 2004; Dai & Zhang 2005; Daigne, Rossi & Mochkovitch 2006). The conclusion has been that $\Phi(L)$ of HL GRBs is generally characterized by a one-component broken power-law (BPL) model with $\rho_{0,\mathrm{HL}} \sim 1\,\mathrm{Gpc^{-3}\,yr^{-1}}$ (e.g. Schmidt 2001; Guetta et al. 2004, hereafter G04; G05). On the other hand, the ρ_0 of LL GRBs inferred from the two detections (GRBs 980425 and 060218) in a decade suggests a much higher local rate than that of HL GRBs, i.e. $\rho_{0,\mathrm{LL}} = 100$–$1000\,\mathrm{Gpc^{-3}\,yr^{-1}}$ (Coward 2005; Cobb et al. 2006; Pian et al. 2006; Soderberg et al. 2006; Chapman et al. 2007; Liang et al. 2007). G04 propose an extension to the lower luminosities which would increase $\rho_{0,\mathrm{HL}}$ from roughly 1.1 to $10\,\mathrm{Gpc^{-3}\,yr^{-1}}$, at roughly $10^{48}\,\mathrm{erg\,s^{-1}}$. This local rate, however, even extrapolated down to $10^{45}\,\mathrm{erg\,s^{-1}}$ is not sufficiently large to produce the observed LL events. This was the main motivation of the two-component model in our previous analysis (Liang et al. 2007, see also Coward 2005; Le & Dermer 2007). The analysis with the z-known sample makes an arguable case (Liang et al. 2007), but is by no means conclusive (cf. G07).

In this paper, we extend our previous analysis to include a more complete set of observational constraints. In particular, we introduce the important BATSE and *Swift* $\log N - \log P$ distribution criteria along with the previously considered multiple criteria involving the z-known sample (one-dimensional z distribution, one-dimensional L distribution, two-dimensional $z - L$ distribution and the observed number ratio of HL versus LL GRBs). Although the number of LL GRBs remains the same, the z-known sample has grown since our last analysis in Liang et al. (2007), a firmer conclusion drawn in this paper is largely due to the additional observational criterion included in this analysis. In order to confront the multiple criteria with different LF models and a wide range of LF parameters, we utilize a series of Monte Carlo simulations (MCSs). Instrument observational selection effects are difficult to model, and we introduce some empirical formulae to roughly reflect gamma-ray detector trigger sensitivity and the selection effect of redshift measurement. Various models are presented in Section 2. Our simulation results are shown in Section 3, and the conclusions and discussion are presented in Section 4. The concordance cosmology with parameters $H_0 = 71\ \mathrm{km\ s^{-1}\ Mpc^{-1}}$, $\Omega_{\mathrm{m}} = 0.3$ and $\Omega_\Lambda = 0.7$ is assumed throughout.

Throughout the paper, we do not touch on another distinctly different group of bursts, namely short-hard bursts (Kouveliotou et al. 1993), or more general type I (see e.g. Zhang et al. 2007 for a discussion of the multiple criteria needed to classify GRBs) bursts, which are found to be consistent with the compact star merger origin (Barthelmy et al. 2005; Berger et al. 2005c; Fox et al. 2005; Gehrels et al. 2005, and see Mészáros 2006; Nakar 2007; Zhang 2007 for reviews). The analysis of these GRBs applying the same technique will be presented elsewhere.

2 MODELS

2.1 Number of detectable GRBs with an instrument

Assuming that the GRB rate at redshift z is $R_{\mathrm{GRB}}(z)$ (number of GRBs per unit time per unit volume), the number of GRBs happening per unit (observed) time in a comoving volume element $\mathrm{d}V(z)/\mathrm{d}z$ is

$$\frac{\mathrm{d}N}{\mathrm{d}t\,\mathrm{d}z} = \frac{R_{\mathrm{GRB}}(z)}{1+z}\frac{\mathrm{d}V(z)}{\mathrm{d}z}, \tag{1}$$

where the $(1+z)$ factor accounts for the cosmological time dilation, and $\mathrm{d}V(z)/\mathrm{d}z$ is given by

$$\frac{\mathrm{d}V(z)}{\mathrm{d}z} = \frac{c}{H_0}\frac{4\pi D_L^2}{(1+z)^2\left[\Omega_{\mathrm{M}}(1+z)^3+\Omega_\Lambda\right]^{1/2}} \tag{2}$$

for a flat Λcold dark matter (ΛCDM) universe. The observed GRB/supernovae connection suggests that the GRB rate could roughly trace the star formation history.[3] We adopt a parametrized GRB rate model proposed by Porciani & Madau (2001),

$$R_{\mathrm{GRB}} = 23\rho_0\frac{e^{3.4z}}{e^{3.4z}+22.0}, \tag{3}$$

or by Rowan-Robinson (1999),

$$R_{\mathrm{GRB}} = \rho_0\begin{cases}10^{0.75z} & z<1\\ 10^{0.75z_{\mathrm{peak}}} & z>1,\end{cases} \tag{4}$$

where z_{peak} is the redshift at which the redshift distribution reaches its maximum (after which it plateaus), taken here as 1.

Supposing the GRB LF is $\Phi(L)$, the number of GRBs per unit time at redshift $z \sim z + \mathrm{d}z$ and luminosity $L \sim L + \mathrm{d}L$ is given by

$$\frac{\mathrm{d}N}{\mathrm{d}t\,\mathrm{d}z\,\mathrm{d}L} = \frac{R_{\mathrm{GRB}}(z)}{1+z}\frac{\mathrm{d}V(z)}{\mathrm{d}z}\Phi(L). \tag{5}$$

Considering an instrument with energy band $[e_1, e_2]$ having a flux threshold F_{th} and an average solid angle Ω for the aperture flux, the number of the detected GRBs during an observational period of T should be

$$N = \frac{\Omega T}{4\pi}\int_{L_1}^{L_2}\Phi(L)\mathrm{d}L\int_0^{z_{\max}}\frac{R_{\mathrm{GRB}}(z)}{1+z}\frac{\mathrm{d}V(z)}{\mathrm{d}z}\,\mathrm{d}z, \tag{6}$$

where $z_{\max}$ for a given burst with luminosity L is determined by the instrumental flux threshold F_{th} through $F_{\mathrm{th}} = L/4\pi D_L^2(z_{\max})k$.

[3] More recently, some authors suggested that the observed GRB rate at high redshift is higher than the star formation rate (SFR) (Cen & Fang 2007; Daigne et al. 2006; Kistler et al. 2007; Li 2007). We will explore various redshift-dependent effects in a future work.

The k factor corrects the observed flux in an instrument band to bolometric flux in the burst rest frame (1–10^4 keV in this analysis),

$$k = \frac{\int_{1/(1+z)}^{10^4/(1+z)} EN(E)\,\mathrm{d}E}{\int_{e_1}^{e_2} EN(E)\,\mathrm{d}E}, \tag{7}$$

where $N(E)$ is the photon spectrum of GRBs. It is generally fitted with a joined PL (the Band function; Band et al. 1993) characterized with photon indices Γ_1 and Γ_2 before and after a break at E_0. The peak energy of the νf_ν spectrum is given by $E_\mathrm{p} = E_0(2 + \Gamma_1)$. It was shown that $\Gamma_1 \sim -1, \Gamma_2 \sim -2.3$ and $E_\mathrm{p} \sim 250$ keV for a typical GRB (Preece et al. 2000). In our analysis, the luminosity extends over 10 orders of magnitude ($[10^{45}, 10^{55}]$ erg s^{-1}). According to the Amati relation (Amati et al. 2002; Liang & Dai 2004), more luminous bursts have a higher E_p, indicating that we cannot adopt a uniform E_p for all the bursts in our analysis. Liang et al. (2004) derived

$$E_\mathrm{p}/200\,\mathrm{keV} = C(L/10^{52}\ \mathrm{erg\ s^{-1}})^{1/2}, \tag{8}$$

where C is randomly distributed in [0.1,1]. We obtain E_p with equation (8) for each burst and assume $\Gamma_1 \sim -1$ and $\Gamma_2 \sim -2.3$ for all bursts.

With the spectral information, one can make the k correction and get the observed peak energy flux and peak photon flux by

$$F = \frac{L}{4\pi D_L^2 k} \tag{9}$$

and

$$P_\mathrm{ph} = \frac{F\int_{e_1}^{e_2} N(E)\,\mathrm{d}E}{\int_{e_1}^{e_2} EN(E)\,\mathrm{d}E}, \tag{10}$$

respectively.

2.2 Luminosity functions

Attempts to determine $\Phi(L)$ of long GRBs have been made by some authors, through fitting the $\log N - \log P$ or V/V_max distributions observed by *Compton Gamma-ray Observatory (CGRO)*/BATSE (Schmidt 2001; Lloyd-Ronning et al. 2002; Norris 2002; Stern et al. 2002; G05), and generally characterize $\Phi(L)$ with a single power law or with a BPL within a given luminosity range $[L_1, L_2]$, i.e.

$$\Phi(L) = \Phi_0 \left(\frac{L}{L_b}\right)^{-\alpha} \tag{11}$$

or

$$\Phi(L) = \Phi_0 \left[\left(\frac{L}{L_b}\right)^{\alpha_1} + \left(\frac{L}{L_b}\right)^{\alpha_2}\right]^{-1}, \tag{12}$$

where Φ_0 is a normalization constant to assure $\int_{L_1}^{L_2} \Phi(L)\,\mathrm{d}L = 1$. The local GRB rate, $\rho_0 = R_\mathrm{GRB}(z = 0)$, is in principle defined to include GRBs with all luminosities. In practice, since observations cannot probe the full LF, the ρ_0 value constrained by the data is usually related to a lowest luminosity L_1. The value of ρ_0, therefore, is a function of L_1. For a single power-law LF (equation 11) with $\alpha > 1$, one has $\rho_0(L > L_1) \propto L_1^{-(\alpha-1)}$, suggesting that a lower L_1 would give rise to a larger observed $\rho_0(L > L_1)$. For a BPL LF (equation 12) with $\alpha_1 < 1$ and $\alpha_2 > 1$, on the other hand, integration suggests that $\rho_0(L > L_1) \sim \rho_0(L > L_b)$ which is essentially independent of L_1. Thus fixing L_b would usually fix ρ_0 in the BPL models. In the past, the LF of HL GRBs was found to have a break around $L_b \sim 10^{50}$ erg s^{-1}, with the value of ρ_0 related to L_b. In our analysis, the local rate is evaluated at a lower-luminosity cut-off for all models, although the value is determined by either L_1 or $L_{b,\mathrm{LL}}$ depending on the forms of LF adopted. These are summarized in Table 1.

2.3 Instrument threshold and detection biases

In order to check if a simulated burst is detectable with a given instrument, the simulated burst is screened with the instrument threshold. The *CGRO*/BATSE was triggered by energy-dependent count rate (Band 2003). We take a moderate sensitivity for *CGRO*/BATSE at 50–100 keV band as $F_\mathrm{th}^\mathrm{BATSE} \sim 10^{-7}$ erg cm^{-2} s^{-1}, roughly corresponding to 0.2 ph cm^{-2} s^{-1} for a typical GRB.

The Burst Alert Telescope (BAT) instrument on board *Swift* operates with an image trigger mechanism. The sensitivity of an event depends on many complicated factors and in principle should be treated on the case-by-case basis. For the purpose of this paper, we adopt an approximate formula of Sakamoto et al. (2007),

$$F_\mathrm{th} \sim (5.3 \times 10^{-9}\,\mathrm{erg\,cm^{-2}\,s^{-1}}) f^{-1} t_{90}^{-0.5}, \tag{13}$$

where f is the partial coded fraction and t_{90} is the burst duration. The larger the burst duration, the more sensitive the instrument. Bursts with $F > F_\mathrm{th}$ can be in principle detected. Observationally, the 'peak fluxes' (and therefore the 'peak luminosities') are usually adopted to denote for the brightness of the bursts, which are on average five times above the average fluxes (Sakamoto, private communication). To compensate this effect, we hereafter adopt an effective threshold condition which is five times larger than equation (13) in our peak–luminosity analyses. Since HL GRBs have a typical duration of 20 s, we adopt a rough constant threshold flux of $F_\mathrm{th,eff} \sim 1.2 \times 10^{-8}$ erg cm^{-2} s^{-1} for the analyses of HL GRBs. As shown by Norris et al. (2005), LL GRBs tend to have longer pulse duration. GRB 060218, for example, has a duration longer than 2000 seconds (Campana et al. 2006; Liang et al. 2006). In our analysis we adopt various discrete values of BAT sensitivities, not exceeding a 500 s

Table 1. Single-component LF models.

Model	Type[a]	α[b]	β[c]	L_B[d]	L_1[e]	L_2[f]	ρ_0[g]	$p_\mathrm{KS,z}$	$p_\mathrm{KS,L}$	$p_\mathrm{KS,t}$
G04	SPL	−0.7	–	–	0.5	500	1.1	0.002 34	0.004 03	9.4×10^{-6}
G04 (2)	BPL	−0.1	−0.7	0.5	0.005	500	10	0.000 18	0.000 22	3.96×10^{-8}
G05 (P&M)[k]	BPL	−0.1	−2.0	71	$71/\Delta_1$[h]	$71\Delta_2$	0.1	1.23×10^{-9}	1.95×10^{-7}	2.4×10^{-14}
G05 (RR)	BPL	−0.1	−2.0	71	$71/\Delta_1$	$71\Delta_2$	0.1	8.1×10^{-12}	2.6×10^{-9}	2.1×10^{-20}
G07	SPL	−1.6	–	–	0.5	500	1.1	1.14×10^{-24}	2.24×10^{-19}	2.6×10^{-43}
G07 (2)	SPL	−1.6	–	–	0.005	500	200	N/A	N/A	N/A
G07 (3)	SPL	−1.6	–	–	5×10^{-4}	500	200–1800[j]	N/A	N/A	N/A

Notes. (a) SPL = simple power law; BPL = broken power law; (b) power-law index; (c) for BPL models, power-law index after the break luminosity; (d) break luminosity for BPL; (e) lower-luminosity cut-off in units of 10^{50} erg s^{-1}; (f) HL cut-off in units of 10^{50} erg s^{-1}; (g) local GRB rate in units of Gpc^{-3} yr^{-1}; (h) $\Delta_1 = 30$, $\Delta_2 = 10$ (see G05); (j) estimation from BATSE data, corrected to 110–1200 Gpc^{-3} yr^{-1} for BAT constraints (see Guetta & Della 2007) and (k) star-forming rate model, Porciani and Madau (P&M) or Rowan-Robinson (RR).

duration (i.e. 4.7×10^{-10} erg cm^{-2} s^{-1}), to screen the simulated LL GRBs.

Theoretically, a GRB could be detectable if $F > F_{\rm th,eff}$. Note that a large fraction of detectable events with F close to $F_{\rm th,eff}$ may not trigger the instrument. This fact was observed in *CGRO*/BATSE. An off-line scan found a large number of non-triggered GRBs in the BATSE catalogue, most of them are near the instrument threshold (Stern et al. 2001). Our simulations, by not adopting a threshold for the $\log N - \log P$ distribution, have an advantage in deciphering the intrinsic low-photon flux end of the distribution, which may be tested in the future by more sensitive detectors such as Joint Astrophysics Nascent Universe Satellite (JANUS) (Roming et al. 2008) and Energetic X-ray Imaging Survey Telescope (EXIST) (Grindlay et al. 2006).

In our analysis we also compare the simulated sample with the redshift-known GRB sample. This sample suffers many observational biases (Bloom et al. 2001; Butler et al. 2007), including position localization, optical detection and line detection. The trigger probability of a burst with a flux close to the instrument threshold tends to be low, as seen in BATSE. Near-threshold GRBs tend to have fainter optical afterglows, which severely bias against their redshift measurements. It is difficult to fully incorporate all these biases into the simulation. We simply model the redshift detection probability of a simulated burst based on an empirical formula,

$$p(F) = \left(1 - \frac{F_{\rm th}}{F}\right)^{\kappa}, \tag{14}$$

where κ is a free parameter. Our analyses show that $\kappa \sim 7$ is necessary to eliminate the overproduction of bursts near the sensitivity threshold. Equation (14) is not highly sensitive on the value of κ, whose most notable effect is on bursts near the threshold. As the value of κ is decreased, most bursts appear near the threshold and below the band of observed bursts, significantly decreasing the significance of the correlation between the simulated and observed bursts. We note that the correlation between gamma-ray and optical luminosities is not a strong one (e.g. Liang & Zhang 2006; Nardini et al. 2006; Kann et al. 2007; Nysewander, Fruchter & Pe'er 2008), and that determination of redshift is easier in some ranges than others. All these make the selection effects more complicated than the simple parametrization such as equation (14). None the less, without simulating the optical luminosities, here we take a simple form for the sake of simplicity, which can effectively screen LL bursts without affecting the bursts significantly above the threshold.

3 MONTE CARLO SIMULATIONS AGAINST OBSERVATIONS

We place constraints on the parameters of $\Phi(L)$ and $R_{\rm GRB}$ through comparing our simulations with observations. The primary criterion to judge the parameters is that the simulated $\log N - \log P$ distribution should match the data. The detection number of an instrument in a given observation period should roughly match the observations. *CGRO*/BATSE and *Swift*/BAT established two uniform samples that can constrain the parameters with the detection event number and the fits to the observed $\log N - \log P$ distributions. The size of the mock GRB sample for a given instrument accumulated in a period T is obtained by equation (6). *CGRO*/BATSE recorded 1637 triggered long GRB events during 9.1 operation years (4B catalogue; Paciesas et al. 1999), and *Swift*/BAT was triggered by ∼300 GRBs during the first three years of operation.[4] We regard all detectable Type II GRB events that could trigger BAT. Therefore, a set of the parameters can be obtained by adjusting the parameters that make the detectable event numbers with BATSE and BAT could be 2176 events in 9.1 yr (1393 triggered and 874 non-triggered) and $N = 300$ in 3 yr, respectively, and the observed $\log N - \log P$ with the two instruments that match our simulations. We measure the consistency between observations and our simulations by a Kolmogorov–Smirnov (KS) test, resulting in a probability $p_{\rm KS}$ (Press et al. 1999). The larger $p_{\rm KS}$ suggests a more significant consistency.

The second criterion to judge the parameters is the constraints from the redshift-known sample and the detections of LL GRBs. The current GRB sample with redshift measurements has ∼100 GRBs and only two confirmed detections of LL GRBs. They were detected by different instruments. Although the sample is not homogeneous for statistics, the parameters of $\Phi(L)$ and $R_{\rm GRB}$ are subject to the constraints from this sample, especially when we take the LL GRBs into account (Liang et al. 2007). First, the detection ratio of LL GRBs to HL GRBs should be ∼1:300 as observed by BAT in three years. Secondly, both the simulated one-dimensional distributions of L and z and the GRB distribution in the $(L - z)$ plane should roughly match the observations. We therefore simulate a subsample of GRBs that have redshift measurement based on the probability of redshift measurement (equation 14) from simulated GRB sample for BAT. We measure the one-dimensional L and z distribution with the KS test, and then combine the distributions in order to place more rigorous constraints. We compare two-dimensional contributions in the $L - z$ plane and measure the consistency of the simulated sample to the observational data with $p_{\rm KS,t} = p_{\rm KS,L} \times p_{\rm KS,}z$.

With the criteria described above, we adjust the model parameters and simulate a large sample of GRBs and filter them with a given instrument threshold without considering the cosmological evolution of $\Phi(L)$, stopping the simulations when a subsample of 150 detectable bursts are reached. Our simulation procedure is summarized as follows.

First, we simulate a burst that is characterized with L at redshift z, GRB(L, z). Both quantities are simulated separately with the probability distributions derived from equation (1) and $\Phi(L)$ (one of equations 11–12).

Secondly, we calculate the $E_{\rm p}$ of a mock GRB with equation (8), and its F and $P_{\rm ph}$ from equations (9) and (10), respectively. The simulated GRB is then screened with the threshold condition $F > F_{\rm th}$.

Thirdly, we simulate a redshift-known subsample from the flux cut-off mock sample with equation (14).

In each of the following sections, we will try different LF models and compare the simulations with the observations.

3.1 Simple power-law model

The first model considered is the simple power-law model (equation 11). This scenario has been extensively studied with the BATSE data (see Section 1). G04 investigate this model without considering the LL GRBs. In order to explain the high detection rate of LL GRBs, G07 proposed that the GRB LF is a single PL with a slope $\alpha = 1.6$ and $\rho_0 = 1.1$, 200 or (200–1800) Gpc^{-3} yr^{-1} depending on which lower-luminosity cut-off was used, $5 \times 10^{49}, 5 \times 10^{47}$ or 5×10^{46} erg s^{-1}, as summarized in Table 1. We make simulations with this model and adopt the parameters from Guetta & Della Valle (2007) and Guetta et al. (2004). The simulated results of these models are shown in Figs 1–4. We first compare the simulated results to the $\log N - \log P$ distribution observed by BATSE. In general, as far as HL GRBs are concerned, the model is able to reproduce a

[4] We do not include those non-triggered events (Schmidt 2004).

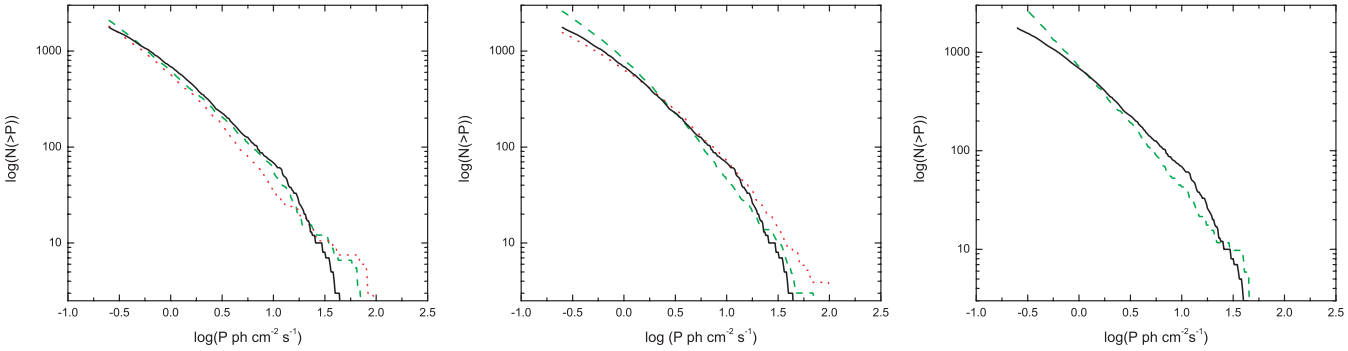

Figure 1. One-LF model fits to BATSE $\log N - \log P$ distribution. The solid line (black) denotes the observed BATSE $\log N - \log P$ distribution in each panel. From left to right-hand panels (a–c), we have the models from G04 (G04 (green, dash); G04(2), (red, dotted)) G05 (P&M (green, dash)); RR (red, dotted) and G07 with the largest $L_{\rm min}$. The first two models (G04, G05) can roughly reproduce the observation, while the last model (G07) is ruled out by the data. The observed BATSE distribution is the solid black curve in all panes.

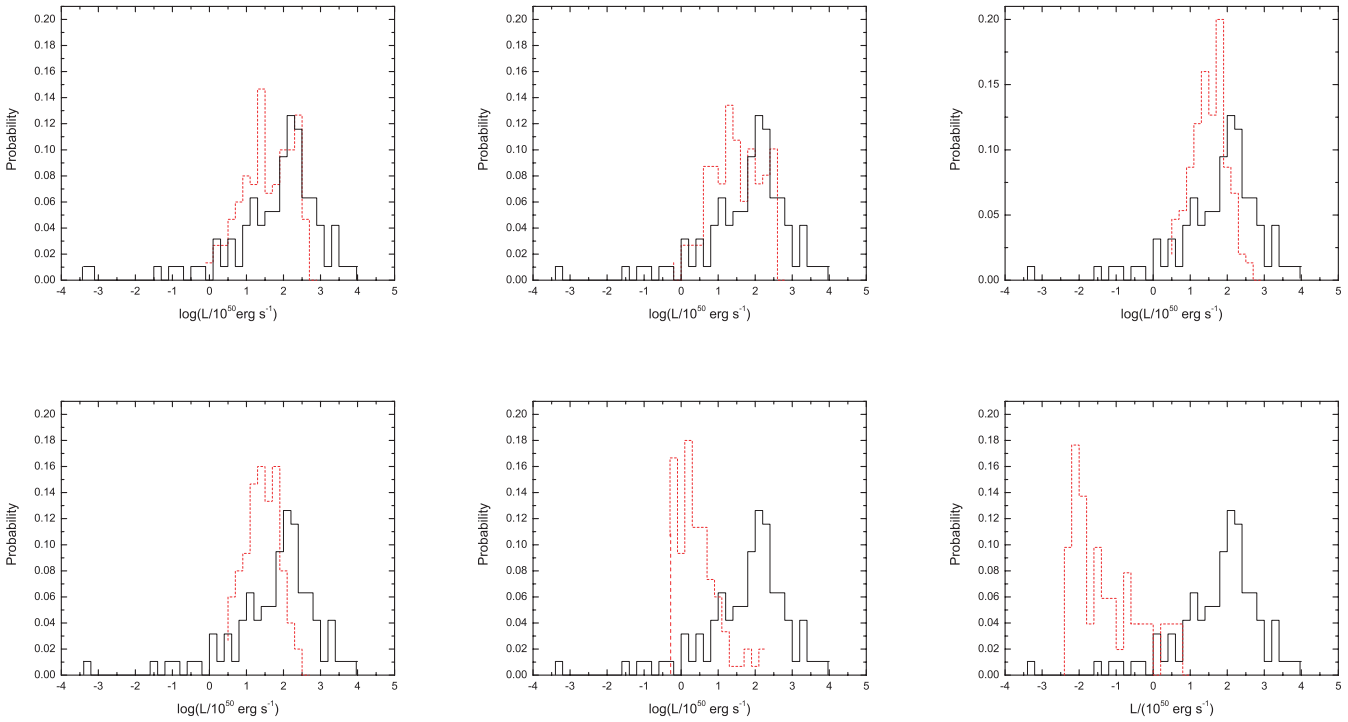

Figure 2. The one-dimensional luminosity distributions of various single-component LF models. The dashed curves (red) are the simulated results, while the solid curves (black) are the observed results for the redshift-known sample. Model parameters can be found in Table 1. The LF forms are, from left to right-hand panels, G04, G04(2), G05 (P&M), G05 (RR), G07, G07(2).

good comparison to the $\log N - \log P$ (Figs 1a and b). However, in order to accommodate LL GRBs, modifications of the LF parameters are needed. The revised model (G07), although able to account for the event rate of LL GRBs, deviates from the observed BATSE $\log N - \log P$ distribution significantly (Fig. 1c).

The simulated distributions of L, z and $L - z$ in a two-dimensional plane are shown in Figs 2–4 along with the observational results. Without considering the LL GRBs, the models of G04 can roughly produce the observed one-dimensional L and z distributions. The model of G07, however, causes a severe overproduction in bursts of luminosities $\sim 10^{48}$–10^{50} erg s^{-1} at low redshifts and fails to reproduce bursts with $z > \sim 3$ for the largest lower-luminosity cut-off of 5×10^{49} erg s^{-1} (see also Liang et al. 2007). The two-dimensional analysis, shown in Fig. 4, demonstrates this overproduction and makes note of the deficiency of bursts above $\sim 10^{52}$ erg s^{-1} in all models. When LL GRBs are considered, the models of G04 are insufficient since they predict a ρ_0 that is too low to account for the observed LL GRBs. While the modified model by G07 can accommodate a sufficiently low cut-off of $0.1 L_{980\,425}$, the steep slope and low cut-off cause a large deviation from the observed $\log N - \log P$ distribution as discussed above.

3.2 Broken power-law model

A single power-law LF model encounters great difficulty in simultaneously reproducing the observed HL-/LL-GRB populations and the BATSE $\log N - \log P$ distributions. Therefore, we try the BPL LF model (equation 12), also discussed by G04 and G05. The

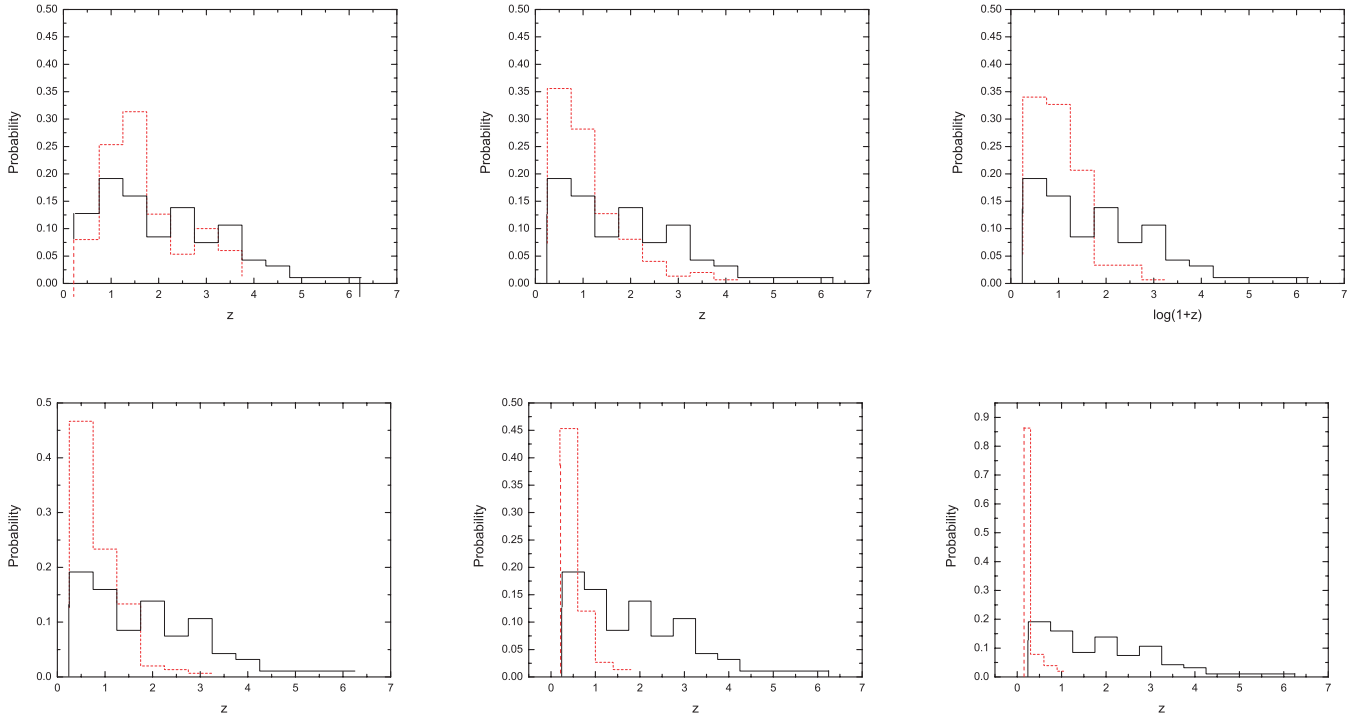

Figure 3. The one-dimensional redshift distributions of various single-component LF models. The dashed curves (red) indicate simulated results, while the solid curves (black) indicate the observed results for the redshift-known sample. The LF forms are, from left to right-hand panels, G04, G04(2), G05 (P&M), G05 (RR), G07, G07(2).

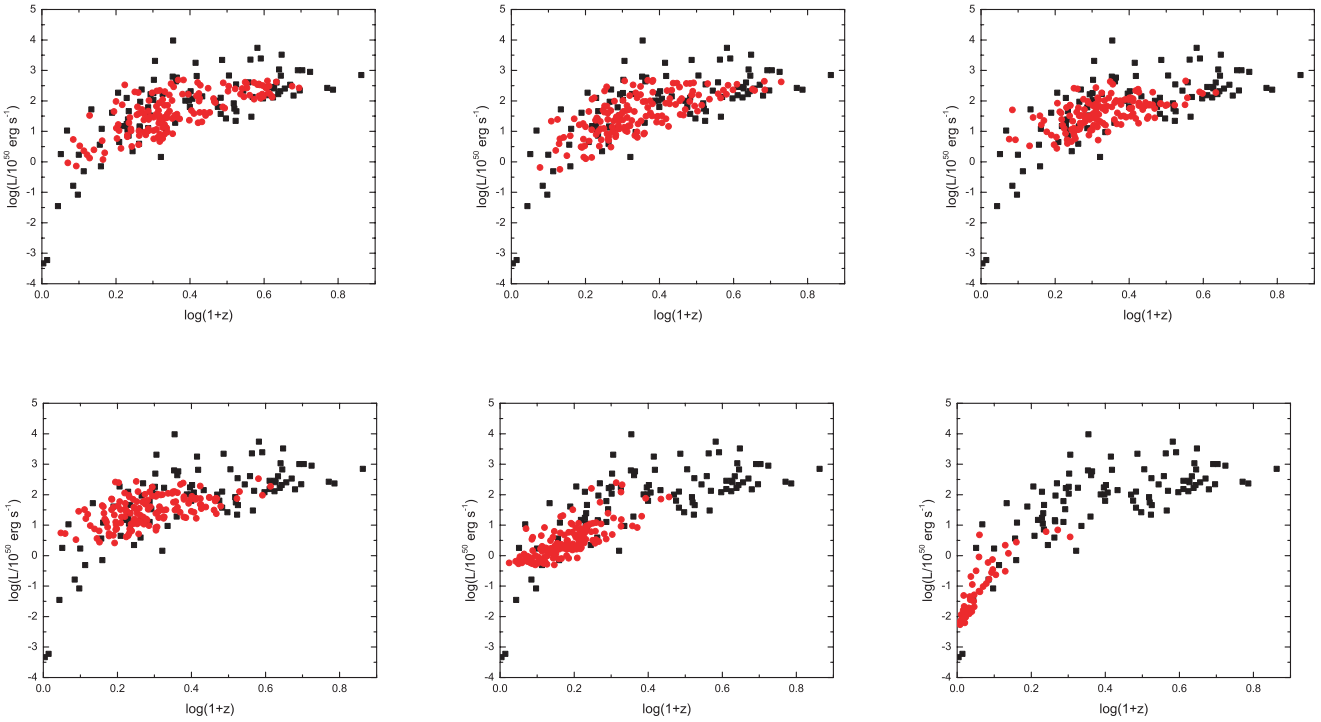

Figure 4. Two-dimensional luminosity–redshift distributions of various single-component PL models. The filled squares (black) are the observed redshift-known sample in the $z - L$ plane, while the filled circles (red) are the simulation results for various models. The LF forms are, from left to right-hand panels, G04, G04(2), G05 (P&M), G05 (RR), G07, and G07(2). None of these models is able to reproduce the observed distribution satisfactorily.

results of which are also shown in Figs 1–4. The BPL model of G04 provides a distribution that peaks at around $z \sim 1$, matching observations, as well as producing a similar number of bursts all around. As the parameters of the BPL are shifted for G05, the peak remains similar although the distribution becomes narrower. Apparently, these results are similar to that of the simple power-law model and cannot explain both HL and LL GRBs and the $\log N - \log P$ distributions.

3.3 Combined broken power-law model: LL GRBs as a distinct GRB population

Coward (2005) and Liang et al. (2007) proposed that LL GRBs could be from a unique GRB population, characterized by LL, less collimation and high local rate as compared to the HL GRBs. With the sensitivity threshold of BATSE and *Swift* BAT, these events are only detectable in a small volume, so that the number of detectable LL GRBs could be low. With more sensitive detectors (e.g. JANUS, Roming et al. 2008; EXIST, Grindlay et al. 2006), one can probe into a larger volume which result in a larger number of detected LL GRBs. To date, only two LL GRBs (GRBs 980425 and 060218) have been well localized. The small number of LL GRBs makes statistical testing of this population alone inaccurate. However, the high local LL-GRB rate inferred from the detection of GRBs 980425 and 060218 and the deficit of the observed GRBs with median luminosity ($10^{48} \sim 10^{49}\,\mathrm{erg\,s^{-1}}$) at redshift $0.1 \sim 0.5$ place strong constraints on the LF of this GRB population. It is unlikely that the lack of intermediate-redshift GRBs is the consequence of some selection effects. Since we are analysing the intrinsic luminosities (rather than the observed fluxes), the deficit should not be related to an instrumental threshold effect, which requires that the LL GRBs would diminish along with the intermediate-luminosities GRBs. A redshift-dependent selection effect would require that there is a strong correlation between burst luminosity and redshift, which is not discovered from the data. We therefore conclude that the observations imply an intrinsic feature in the LF. Liang et al. (2007) suggested that the global GRB LF can be modelled with two components: a smoothed BPL for each population. We elaborate this two-component model with our simulations.

The simulated GRBs cover a luminosity interval of $L = 10^{45}$–$10^{55}\,\mathrm{erg\,s^{-1}}$ and a redshift interval of $z = 0$–10. The values of luminosity and redshift assigned are subjected to the detector conditions described above, until a subset of 300 bursts (similar to the observed number of these types of bursts by *Swift*) is achieved. We then constrain the two-component LF parameters with the following procedure. First, we vary the parameters for the HL-GRB LF and compare with the observed one-dimensional L and z distributions as well as the two-dimensional $(L - z)$ distributions. Since the results are not sensitive to the value of $\alpha_{2,\mathrm{HL}}$, we fix it at 2.5, and search for high-likelihood parameters in the $L_b - \alpha_{1,\mathrm{HL}}$ space using KS probability contours (Fig. 5). This leads to high-probability concentrations in a variety of spots. We then use the $\log N - \log P$ criterion to pin down the best parameter space.

Next, we constrain the LL-GRB component parameters using the one- and two-dimensional distributions as well as the relative ratio of the observed HL and LL GRBs. In order to address the number of simulated bursts that pass the threshold conditions, it is necessary to understand how each population was controlled. The number of LL bursts created was directly proportional to the number of HL bursts created by the ratio of the local rates for each type of burst. The number of LL iterations was prescribed by

$$N_{\mathrm{LL}} = N_{\mathrm{HL}} \frac{\rho_{0,\mathrm{LL}}}{\rho_{0,\mathrm{HL}}}. \tag{15}$$

A change in either rate will result in different amounts of each type of burst created, which then affects the final distributions and observable number of bursts. It is necessary to note that the observable ratio of about 300:1 (HL:LL) bursts is for all triggered bursts, not just the redshift-known subset. Therefore, the redshift-measurement probability condition (equation 14) need not be applied to the bursts since the purpose of this addition was to simulate the redshift measurement bias.

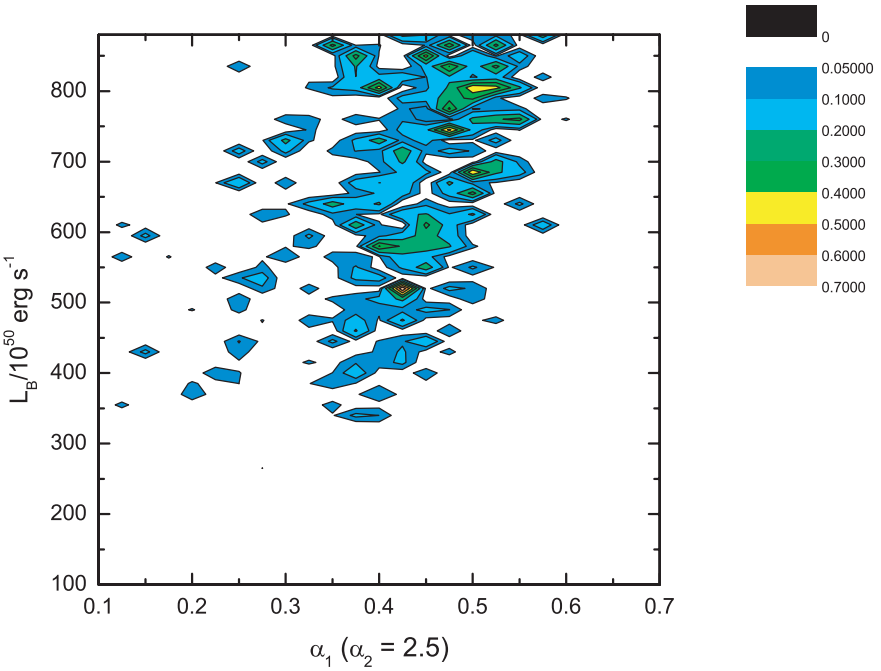

Figure 5. Two-dimensional $p_{\mathrm{KS,t}}$ contour as a function of $\alpha_{1,\mathrm{HL}}$ and L_b at $\alpha_2 = 2.5$.

Analysis of the two-component LF model shows promising results and constraints on the LF and local rate of both HL and LL bursts. It is found that the parameter set $(\alpha_{1,\mathrm{HL}}, \alpha_{2,\mathrm{HL}}, L_b) = (0.425, 2.5, 5.2 \times 10^{52}\,\mathrm{erg\,s^{-1}})$ gives a reasonable fit to both the $L - z$ constraints and the $\log N - \log P$ distribution, producing a strong peak in $L - z$ probability and fit to the $\log N - \log P$ distribution. For completeness, we also consider two other sets of parameters, $(\alpha_{1,\mathrm{HL}}, \alpha_{2,\mathrm{HL}}, L_b) = (0.5, 2.5, 8 \times 10^{52}\,\mathrm{erg\,s^{-1}})$ and $(0.475, 2.5, 7.2 \times 10^{52}\,\mathrm{erg\,s^{-1}})$, which correspond to the second highest peak in $\alpha_1 - L_B$ space, and a sample near the centre of the maximum values of the contour. These parameter sets are the combination and result of the first three criteria for constraining the LF parameters, as mentioned in the introduction.

Moving on to the last criterion, the best-fitting parameters give number ratios of roughly 40:1 to 1000:1, depending on the assumed duration (and therefore instrument sensitivity) chosen for the set of bursts as well as the assumed values for the local event rates of both populations. For $\rho_{0,\mathrm{LL}} = 100\,\mathrm{Gpc^{-3}\,yr^{-1}}$ (with $\rho_{0,\mathrm{HL}}$ maintained at 1 $\mathrm{Gpc^{-3}\ yr^{-1}}$), a duration (i.e. t_{90}) of 300 s gives a ratio of 218:1 HL to LL bursts, in general agreement with observation. If the rate for these bursts is increased to 200 or 400 $\mathrm{Gpc^{-3}\ yr^{-1}}$, the durations that give reasonable results drop significantly to 120 and 20 s, respectively. This observable ratio is difficult to gauge, however, due to the few LL GRBs that actually pass the threshold condition for instrument sensitivity and the fact that there could be a range of durations for individual bursts as well as uncertainty in the local rates. A change in both the duration, $\rho_{0,\mathrm{LL}}$ and/or $\rho_{0,\mathrm{HL}}$, will modify the set of parameters that will give the correct ratio, as shown above. For example, if one increases the duration from 120 to 500 s and maintains a rate of 200 $\mathrm{Gpc^{-3}\ yr^{-1}}$, the number of LL bursts detected increases about threefold, significantly lowering the ratio. A similar change in ratio will occur when shifting the values of ρ_0. Small changes in the LF parameters of HL bursts (e.g. $L_B = 6.85 \times 10^{52}\,\mathrm{erg\,s^{-1}}$ modified to $9.85 \times 10^{52}\,\mathrm{erg\,s^{-1}}$) do not significantly affect this ratio. More sensitive detectors (e.g. JANUS, Roming et al. 2008; EXIST, Grindlay 2006) are crucial for the amassing of LL-burst data and will greatly assist determining typical time-scales of these bursts, which affects the sensitivity of the detector, as well as further constrain the relative ratio and in generally improve statistics. The simulated LL component should not significantly affect the bulk of the $L - z$ and the $\log N - \log P$ distributions, but in the meantime gives rise to the desired LL-GRB events. Due to small number statistics, the LL-component parameters cannot be well constrained, especially for $\alpha_{1,\mathrm{LL}}$. In any case, a set of parameters that can best reproduce the data can be obtained, which are summarized in Table 2. Figs 6–9 graphically present the simulated results with the constrained parameters in Table 2 against the observational data, each set of graphs depicting a different constraint. Fig. 6 shows the observed $\log N - \log P$ distributions superimposed with the simulated distributions for the two-component LF model. In addition to the BATSE sample (top curves), we also compare with the *Swift*/BAT sample (lower curves). The observed

Table 2. Two-component LF model parameters.

α_1^{LL}	α_2^{LL}	$L_B^{\mathrm{LL}a}$	$\rho_0^{\mathrm{LL}b}$	α_1^{HL}	α_2^{HL}	L_B^{HL}	ρ_0^{HL}	$p_{\mathrm{KS,t}}{}^c$
0.0	3.5	10^{47}	100	0.425	2.5	5.2×10^{52}	1	0.69
0.0	3.5	10^{47}	100	0.5	2.5	8.1×10^{52}	1	0.474
0.0	3.5	10^{47}	100	0.45	2.5	7.5×10^{52}	1	0.167

Notes. (a) $\mathrm{erg\,s^{-1}}$; (b) $\mathrm{Gpc^{-3}\,yr^{-1}}$; (c) Total KS probability, $p_{\mathrm{KS,t}} = p_{\mathrm{KS,L}} \times p_{\mathrm{KS,z}}$.

Table 3. Observed GRBs data.

GRB ID	z	$\log(L/\mathrm{erg\,s^{-1}})^a$	References
970228	0.695	51.24	1
970508	0.835	51.16	2,3
970828	0.9578	51.52	4
971214	3.42	52.83	5
980326	1.00	52.03	6
980613	1.096	50.16	7
980703	0.966	52.21	8
990123	1.6	53.25	9
990506	1.3	52.63	10
990510	1.619	52.81	11
990705	0.842	51.97	12
990712	0.434	50.56	13
991208	0.706	51.39	14
991216	1.02	53.31	15
000301C	2.03	52.10	16
000418	1.118	52.22	17
000926	2.066	53.34	18
010921	0.45	51.08	19
011121	0.360	51.72	20
011211	2.14	51.42	21
020405	0.69	52.09	22
020531	1.00	52.25	23
020813	1.25	52.79	24
020903	0.25	48.92	25
021004	2.3	51.34	26
021211	1.006	52.69	27, 28
030226	1.98	51.80	29, 30
030323	3.372	53.03	31
030328	1.52	52.31	32,33,34
030329	0.168	51.02	35
030429	2.65	53.35	36
040701	0.2146	49.21	37
040924	0.859	52.37	38
041006	0.716	51.66	39
050126	1.29	51.28	40
050315	1.949	52.00	41
050318	1.44	52.01	42
050319	3.24	52.41	43
050401	2.9	53.39	44
050416	0.6535	51.17	45
050505	4.3	52.95	46
050525	0.606	52.27	47
050603	2.821	53.74	48
050724	0.258	50.23	49
050730	3.97	52.34	50,51
050802	1.71	52.14	52
050820	2.61	52.61	53
050824	0.83	50.59	54
050904	6.29	52.85	55
050908	3.344	52.22	56, 57
051016B	0.9364	51.10	58
051109	2.346	52.54	59
051111	1.55	52.07	60
051221	0.5465	51.61	61
051227	0.714	50.86	62
060115	3.53	52.40	63
060124	2.296	51.91	64
060206	4.04998	53.01	65
060210	3.91	53.01	66
060614	0.125	50.25	67
980425	0.0085	46.67	68
060218	0.0331	46.78	69
031203	0.105	48.55	70
050826	0.297	49.69	71

Table 3 – *continued*

GRB ID	z	$\log(L/\mathrm{erg\,s^{-1}})^a$	References
050922C	2.199, 2.198	52.83	72, 104
060418	41.489	52.24	73, 74
060502	1.51	51.80	75
060510B	4.9	52.43	76
060512	0.4428	49.85	77
060522	5.11	52.37	78
060526	3.21, 3.221	52.46	79, 104
060604	2.68	51.48	80
060605	3.78	52.18	81
060607	3.082	52.46	82
060707	3.425	52.19	83
060714	2.71, 2.711	52.13	84, 104
060904B	0.703	51.05	85
060906	3.686	52.53	86
060912	0.937	51.79	87, 105
060926	3.208	52.11	88
061004	0.3	52.60	106
061007	1.262	54.01	90
061110	0.757	50.35	91
061110B	3.44	53.52	92
061121	1.314	52.73	93
061222B	3.4	52.32	94
070110	2.352	51.64	95
070208	1.165	50.97	96
070306	1.497	52.01	97
070318	0.84	51.13	98
070411	2.954	52.08	99
070506	2.31	51.7661	100
070529	2.4996	52.28	101
070611	2.04	51.56	102
070612	0.617	50.64	103

References: (1) Djorgovski et al. 1997; (2) Bloom et al. 1997; (3) Zharikov et al. 1997; (4) Djorgovski et al. 2001b; (5) Hogg Turner, 1998; (6) Fruchter et al. 2001a; (7) Djorgovski et al. 1999; (8) Djorgovski et al. 1998; (9) Gal et al. 1999; (10) Bloom et al. 2001; (11) Vreeswijk et al. 1999a; (12) Le Floc'h et al. 2002; (13) Galama et al. 1999; (14) Dodonov et al. 1999; (15) Vreeswijk et al. 1999b; (16) Castro et al. 2000; (17) Bloom et al. 2000; (18) Fynbo et al, 2000; (19) Djorgovski et al. 2001a; (20) Infante et al. 2001; (21) Fruchter et al. 2001b; (22) Masseti et al. 2002; (23) Kulkarni et al. 2002; (24) Price et al, 2002; (25) Soderberg et al. 2002; (26) Chornock et al. 2002; (27) Vreeswijk et al. 2003a; (28) Della Valle et al. 2003; (29) Greiner et al. 2003a; (30) Price et al. 2003; (31) Vreeswijk et al. 2003b; (32) Martini et al. 2003; (33) Rol et al. 2003; (34) Maiorano et al. 2006; (35) Greiner et al. 2003b; (36) Weidinger et al. 2003; (37) Kelson, 2004; (38) Wiersema et al. 2004; (39) Price et al. 2004; (40) Berger et al. 2005b; (41) Kelson & Berger, 2005; (42) Berger & Mulchaey, 2005; (43) Fynbo et al. 2005a; (44) Fynbo et al. 2005b; (45) Cenko et al. 2005; (46) Berger et al. 2005a; (47) Foley et al. 2005a; (48) Berger & Becker 2005; (49) Prochaska et al. 2005a; (50) Chen et al. 2005; (51) D'Elia et al. 2005; (52) Fynbo et al. 2005c; (53) Prochaska et al. 2005b; (54) Fynbo et al. 2005d; (55) Kawai et al. 2005; (56) Fugazza et al. 2005; (57) Foley et al. 2005b; (58) Soderberg et al. 2005; (59) Quimby et al. 2005; (60) Hill et al. 2005; (61) Berger Soderberg, 2005; (62) Foley et al. 2005c; (63) Piranomonte et al. 2006; (64) Cenko et al. 2006a; (65) Prochaska et al. 2006; (66) Cucchiara et al. 2006a; (67) Price et al. 2006a; (68) Holland et al. 2000; (69) Mirabal & Halpern 2006; (70) Prochaska et al. 2003; (71) Halpern & Mirabal, 2006; (72) Jakobsson et al. 2005; (73) Vreeswijk & Jaunsen, 2006; (74) Dupree et al. 2006; (75) Cucchiara et al. 2006b; (76) Price, 2006b; (77) Bloom et al. 2006a; (78) Cenko et al. 2006b; (79) Berger & Gladders, 2006; (80) Castro-Tirado et al. 2006; (81) Still et al. 2006; (82) Ledoux et al. 2006; (83) Jakobsson et al. 2006a; (84) Jakobsson et al., 2006b; (85) Fugazza et al. 2006; (86) Vreeswijk et al. 2006; (87) Jakobsson et al. 2006c; (88) D'Elia et al. 2006; (89) Jakobsson et al. 2006d.

Table 3 – *continued*

(90) Osip et al. 2006; (91)Thoene et al. 2006; (92) Fynbo et al, 2006b; (93) Bloom et al. 2006b; (94) Berger, 2006; (95) Jaunsen et al. 2007a; (96) Cucchiara et al. 2007; (97) Jaunsen et al. 2007b; (98) Jaunsen et al. 2007c; (99) Jakobsson et al. 2007; (100) Thoene et al. 2007a; (101) Berger et al. 2007; (102) Thoene et al. 2007b; (103) Cenko et al. 2007; (104) Jakobsson et al. 2006e; (105) Levan et al. 2007 and (106) Jakobsson et al. 2006f.

Notes. (a) The spectral parameters and observed fluences in BAT band are taken from Sakamoto et al. (2007). In order to correct the observed fluence to the $1–10^4$ keV band in the burst rest frame, we derive the E_p of each bursts with the relation between E_p and the spectral PL index (Sakamoto et al. 2007; Zhang et al. 2007) in the BAT band and assume that $\Gamma_1 = -1$ and $\Gamma_2 = -2.3$ for all bursts.

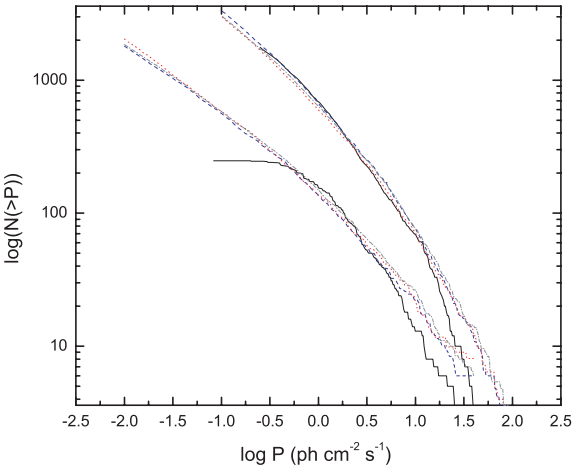

Figure 6. Two-component LF model fits to BATSE (top curves) and *Swift*/BAT (lower curves) $\log N - \log P$ distributions. The solid (black) curves are the observations, the dashed (blue) curves are the best-fitting parameters from the two-dimensional contour, the dotted (red) curves are second peak in the probability distribution and the dash–dotted (grey) curves represent the middle parameters in the maximum of the $p_{\mathrm{KS,t}}$ space (see Table 3 for details).

distributions seem to level off towards the low-photon flux end. However, this is an effect created by the approach to the detection threshold of the particular instrument. The simulated results are not subjugated to such a cut-off, which serves as a prediction of the model for future observations by more sensitive detectors such as JANUS and EXIST. The simulated results are truncated at $0.01\,\mathrm{ph\,cm^{-2}\,s^{-1}}$, roughly 20 times the BATSE sensitivity. The model also slightly overpredicts the number of bursts in the HL end. However, since the number of very HL GRBs is a small fraction of the total number of GRBs, this excess does not significantly worsen the fit to the data (see also Dai & Zhang 2005). The discrepancy might be interpreted as due to small number statistics. In general, the two-component model reproduces the observed $\log N - \log P$ distribution much better than the other models presented in Fig. 1.

Next we consider the one- and two-dimensional z and L distributions whose results are summarized in Figs 7–9. The simulated redshift distribution follows the observed distribution well through high z, except that the observations show a slight overproduction of bursts with $z > 5$. This may be related to the possible evolutionary effects or additional factors (e.g. metallicity) that determine the GRB rate (Cen & Fang 2007; Daigne et al. 2006; Kistler et al.

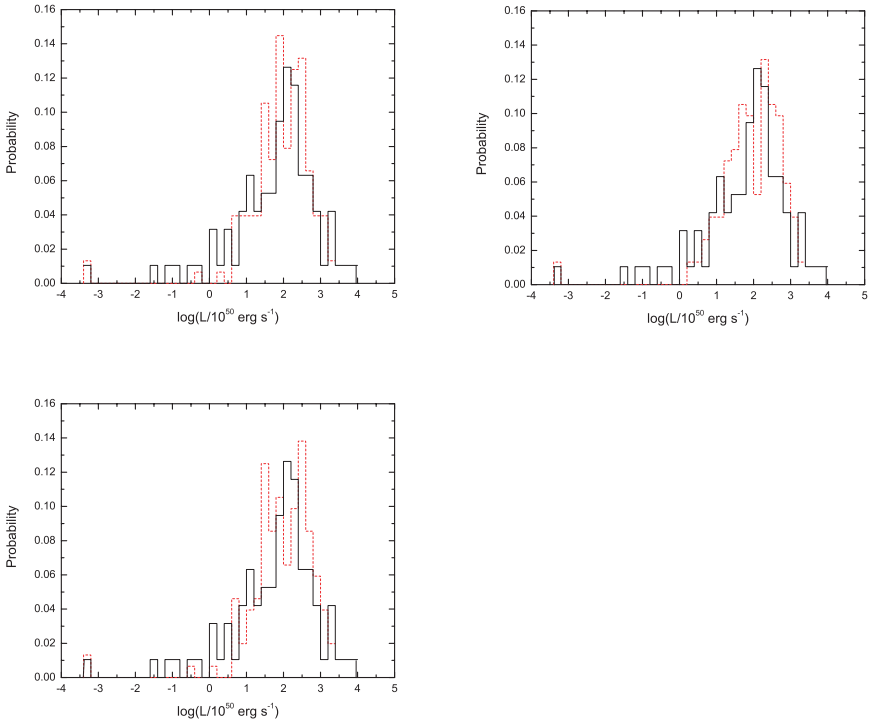

Figure 7. One-dimensional luminosity distribution of simulated GRBs (dashed) generated from the two-component LF model compared to the observed GRBs (solid). The panels correspond to best, intermediate and centre KS probability fits, respectively.

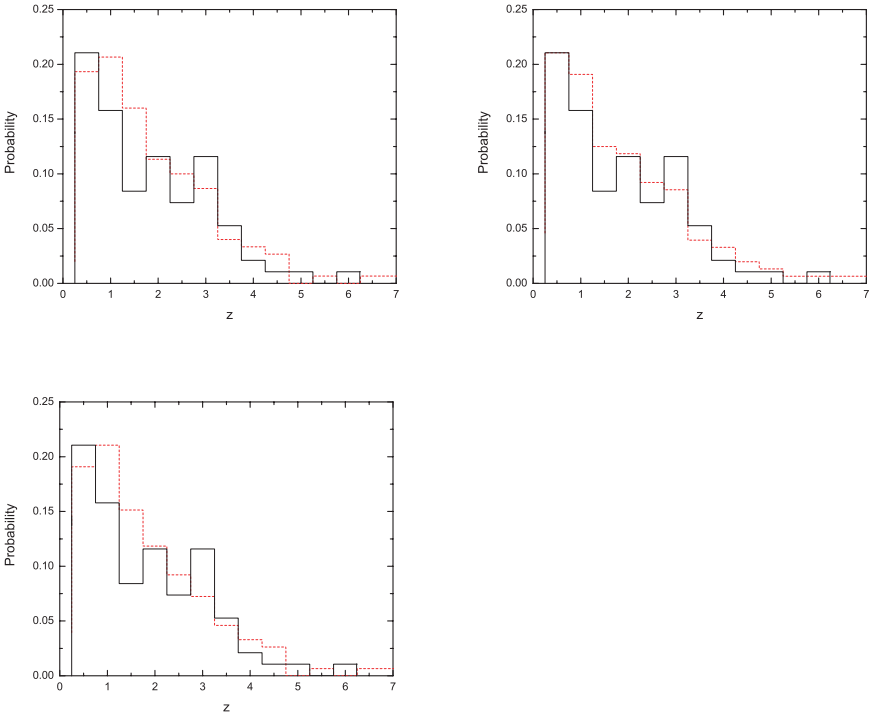

Figure 8. One-dimensional redshift distribution of simulated GRBs (dashed) generated from the two-component LF model compared to the observed GRBs (solid). The panels correspond to best, intermediate and centre KS probability fits, respectively.

2008; Li 2007), which we will fully address in a future work. The simulated one-dimensional luminosity distribution is also similar to the observed distribution, broadly peaking at $\sim 10^{52}$ erg s^{-1}. A slight deficit of bursts below $\sim 10^{50}$ erg s^{-1} is seen in the data. This effect is most likely caused by the assumption of the probability for redshift measurement (equation 14), or perhaps an effect of a neglected redshift dependence (see discussion below). The two-dimensional $\log L - \log z$ distributions are detailed in Fig. 9 and show that

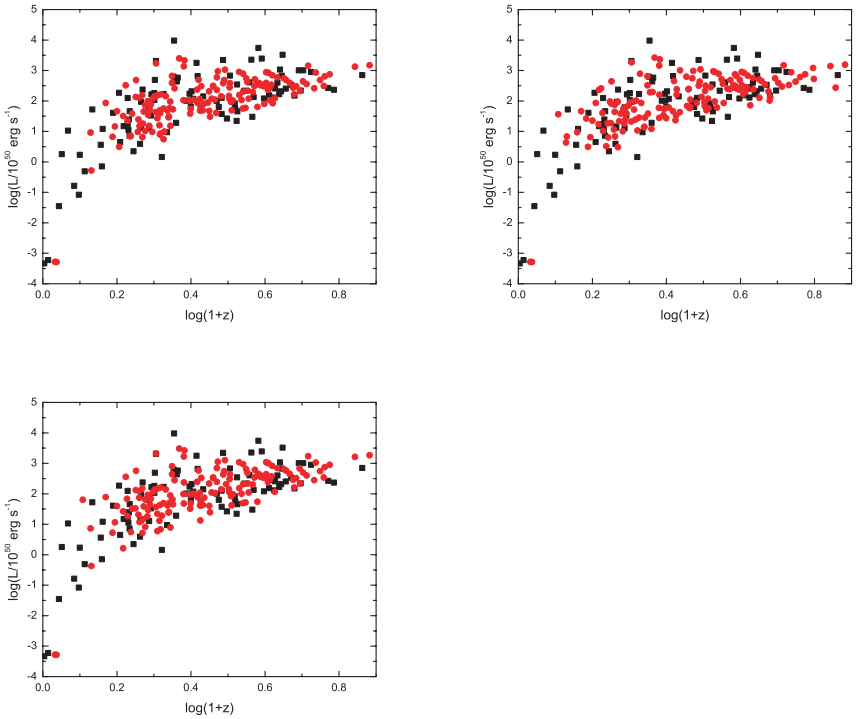

Figure 9. Two-dimensional ($z - L$) graph of simulated bursts from the two-component LF model (red circles) as compared to the observed GRBs (black squares). The panels correspond to best, intermediate and centre KS probability fits, respectively.

the simulated results generally match the band of observed bursts. There is a small underproduction of bursts of 10^{53}–10^{54} erg s^{-1} at intermediate redshifts of $z \sim 3$ as well as below $\sim 10^{50}$ erg s^{-1}. On the other hand, any attempt to increase the number of bursts in this luminosity range would skew the $\log N - \log P$ distribution at the high-photon flux end. A possible cause may be that the fraction of bursts with redshift measurements in this ($L - z$) range may be slightly higher due to the complicated selection effects which are not modelled. The two simulated LL bursts are included in this graph, represented at the lower left-hand corner very near to the observed bursts. The number of HL bursts plotted reflects the bias in measuring redshifts, namely that only ∼20 to 30 per cent of the HL bursts have a measured redshift. LL bursts are assumed to have a nearly 100 per cent redshift detection rate thanks to their proximity.

As mentioned above, intermediate-LF parameters were used in producing Figs 6–9. Finding more sophisticated functional forms of the trigger probability, simulating individual burst time-scales, and/or adding terms that evolve with redshift will most likely increase the overlap of $p_{\mathrm{KS},z}$ and $p_{\mathrm{KS,L}}$ which together constrain the LF parameters. Another factor that influences the KS probability is the size of the sample of observed GRBs used in the analysis. As the *Swift* GRB sample continues to grow, and more bursts are observed with redshift measurements, the statistical possibilities for the analysis will also be increased. To date, a total of 95 bursts have redshift measurements, 54 of those coming from *Swift* localizations.

4 CONCLUSIONS AND DISCUSSION

By utilizing MCSs and various test criteria, we are able to further constrain the form and parameters of the LF of long GRBs. After confronting model results with various observational criteria, including one- and two-dimensional $L - z$ distributions of the redshift-known GRBs and the $\log N - \log P$ distributions of both *CGRO*/BATSE and *Swift*/BAT GRBs, we conclude that various one-component LF models discussed by previous authors (e.g. G04; G05; G07) are insufficient to account for all the data. As the luminosity function parameters are modified to accommodate for the observed LL bursts, these models cause an overproduction of bursts at low and intermediate redshifts that is irreconcilable with the observed distributions. Although a PL or BPL would seem a simple and straightforward solution to the LF problem, our reasoning and analysis imply that a two-component LF model (Coward 2005; Liang et al. 2007) is necessary. The latter model implies an event rate of local LL GRBs of ∼100–400 Gpc^{-3} yr^{-1} at an $L_{B,\mathrm{LL}}$ of $L \sim 10^{47}$ erg s^{-1}, which is much larger than that of HL GRBs (∼1 Gpc^{-3} yr^{-1}). In addition, as mentioned in Liang et al. (2007), the functional form of the LL-bursts LF is quite uncertain, especially below the break luminosity. Most constraints are drawn from the more numerous HL observations, although important information about local rate and break luminosities for both distributions can be drawn simply from the number of LL events detected within the time of *Swift*'s operation. Other effects that add difficulty to the analysis, but are addressed as fully as possible, include the inhomogeneity of the burst sample, redshift detection selection effects and the relatively small sample size.

A recent development that may affect the local rate determination is the serendipitous discovery of a very LL (peak luminosity $\sim 6.1 \times 10^{43}$ erg s^{-1}) X-ray transient, XRF 080109, by *Swift* XRT (Soderberg et al. 2008). This event is associated with SN 2008D. Although it has been suggested that the X-ray emission may be related to shock breakout (Soderberg et al. 2008), the possibility that the X-ray emission is the jet emission from a very LL X-ray flash has been suggested and cannot be ruled out from the data (Li

2008; Xu et al. 2008). In particular, the non-thermal spectrum of XRF 080109 makes it different from the thermal X-ray emission component discovered in XRF 060218, another shock-breakout emission candidate claimed in the literature (Campana et al. 2006). We therefore regard the origin of XRF 080109 inconclusive. If it is indeed a very low luminosity LL GRB, its very high event rate (Soderberg et al. 2008; Xu et al. 2008) is consistent with the conclusion of this paper that LL GRBs form a distinct new component in LF, and the event rate increases to even higher values towards low luminosities. This model also predicts the existence of X-ray flashes in the luminosity range of 10^{44}–10^{46} erg s^{-1} that bridge XRF 080109 and 060218.

The current LL-GRB sample is too small to address whether they follow the same empirical correlations as HL GRBs, such as the lag–luminosity relation (Norris et al. 2005), variability–luminosity relation (Reichart et al. 2001), spectral peak energy–isotropic energy relation (Amati et al. 2002), etc. Apparent discrepancy exists for some (e.g. GRB 980425 as an outlier of the Amati relation), but consistency exists for others (e.g. GRB 060218 satisfies the Amati and lag–luminosity relations; Amati 2006; Liang et al. 2006). On the other hand, these correlations are closely related to the radiation physics, which are not directly related to the central engine and progenitor of the bursts. The GRB fireball picture is very generic. Bursts with different types of progenitors may share the same emission physics and, hence, similar empirical correlations. More data are needed to draw firmer conclusions in this direction.

In the above analysis, we show that this two-component LF model can interpret observations from both *Swift* and *CGRO*/BATSE in various criteria. Although some accommodations have been made to find common ground within all tests employed, these criteria shed light on the LF problem and imply that a two-component LF is necessary. Various effects that are not considered in this work may further affect the luminosity and redshift distribution of the observed bursts. Changes to the form of the SFR appear often in the literature and are essential to the basic assumptions of long GRBs as being associated with the death of massive stars. MCSs provide a useful tool for probing this effect, either as different functional forms of the SFR (Rowan-Robinson 1999; Porciani & Madau 2001; Hopkins & Beacom 2006) or deviations and evolutions with redshift (Kistler et al. 2007). Other effects that might affect the distributions include an evolution of the LF with redshift (Lloyd-Ronning et al. 2002) or a dependence on cosmic metallicity (Li 2007). These processes might provide solutions to the deficit of simulated bursts at HL and high-redshift, since most of these effects produce a larger rate of bursts at high redshift. Consequently, this redshift dependence does not affect the nearby LL population. Understanding how and to what extent each of these processes affects the luminosity and redshift distributions is a necessary next step in the constraints of the LF of GRBs, and we plan to explore them in full in a future work.

ACKNOWLEDGMENTS

We thank T. Sakamoto and N. Butler for important discussions regarding BAT trigger procedure and sensitivity threshold, and P. Jakobsson, R. Chapman for useful communications. This work is supported by NASA under grants NNG05GB67G, NNG05GH92G and the Nevada EPSCoR programme, and by the President's Infrastructure Award from UNLV. FJV acknowledges NASA's Nevada Space Grant. EWL acknowledges the National Natural Science Foundation of China under grant 10463001.

REFERENCES

Amati L., 2006, MNRAS, 372, 233
Amati L. et al., 2002, A&A, 390, 81
Band D. et al., 1993, ApJ, 413, 281
Barthelmy S. D. et al., 2005, Nat, 438, 994
Berger E., 2006, GCN 5962
Berger E., Becker G., 2005, GCN 3520
Berger E., Gladders M., 2006, GCN 5170
Berger E., Mulchaey J., 2005, GCN 3122
Berger E., Soderberg A. M., 2005, GCN 4384
Berger E., Soderberg A. M., 2008, GCN 7159
Berger E. et al., 2005a, GCN 3368
Berger E. et al., 2005b, GCN 3088
Berger E. et al., 2005c, Nat, 438, 988
Berger E. et al., 2007, GCN 6470
Bloom J. S. et al., 1997, GNC3 30
Bloom J. S. et al., 2000, GCN 661
Bloom J. S. et al., 2001, AJ, 121, 2879
Bloom J. S. et al., 2006a, GCN 5217
Bloom J. S. et al., 2006b, GCN 5826
Butler N. et al., 2007, ApJ, 671, 656
Cabrera J. I. et al., 2007, MNRAS, 382, 342
Campana S. et al., 2006, Nat, 442, 1008
Castro S. M. et al., 2000, GCN 605
Castro-Tirado A. J. et al., 2006, GCN 5218
Cenko S. B. et al., 2005, GCN 3542
Cenko S. B. et al., 2006a, GCN 4592
Cenko S. B. et al., 2006b, GCN 5155
Cenko S. B. et al., 2007, GCN 6556
Chapman R. et al., 2007, MNRAS, 382, 21
Chen H. W. et al., 2005, GCN 3709
Chornock R. et al., 2002, GCN 1605
Cobb B. E. et al., 2006, ApJ, 645, L113
Colgate S. A., 1974, ApJ, 187, 333
Coward D. M., 2005, MNRAS, 360, 77
Cucchiara A. et al., 2006a, GCN 4729
Cucchiara A. et al., 2006b, GCN 5052
Cucchiara A. et al., 2007, GCN 6083
Dai X., Zhang B., 2005, ApJ, 621, 875
Daigne F., Mochkovitch R., 2007, A&A, 465, 1
Daigne F., Rossi E., Mochkovitch R., 2006, MNRAS, 372, 1034
D'Elia V. et al., 2005, GCN 3746
D'Elia V. et al., 2006, GCN 5637
Della Valle M. et al., 2003, GCN 1809
Djorgovski S. G. et al., 1997, GCN 289
Djorgovski S. G. et al., 1998 GCN 137
Djorgovski S. G. et al., 1999, GCN 189
Djorgovski S. G. et al., 2001a, GCN 1108
Djorgovski S. G. et al., 2001b, ApJ, 562, 654
Dodonov S. N. et al., 1999, GCN 475
Dupree A. K. et al., 2006, GCN 4969
Foley R. J. et al., 2005a, GCN 3483
Foley R. J. et al., 2005b, GCN 3949
Foley R. J. et al., 2005c, GCN 4409
Fox D. B. et al., 2005, Nat, 437, 845
Fruchter A. et al., 2001a, GCN 1029
Fruchter A. et al., 2001b, GCN 1200
Fugazza D. et al., 2005, GCN 3948
Fugazza D. et al., 2006, GCN 5513
Fynbo J. P. U. et al., 2000, GCN 807
Fynbo J. P. U. et al., 2005a, GCN 3136
Fynbo J. P. U. et al., 2005b, GCN 3176
Fynbo J. P. U. et al., 2005c, GCN 3749
Fynbo J. P. U. et al., 2005d, GCN 3874
Fynbo J. P. U. et al., 2006b, GCN 5809
Gal R. R. et al., 1999, GCN 213
Galama T. J. et al., 1999, GCN 388

Gehrels N. et al., 2005, Nat, 437, 851
Gehrels N. et al., 2006, Nat, 444, 1044
Greiner J. et al., 2003a, GCN 1886
Greiner J. et al., 2003b, GCN 2020
Grindlay J. et al., 2006, AAS Meeting 209, 54.01
Guetta D., Della Valle M., 2007, ApJ, 657, L76 (G07)
Guetta D., Perna R., Stella L., Vietri M., 2004, ApJ, 615, L73 (G04)
Guetta D., Piran T., Waxman E., 2005, ApJ, 619, 412 (G05)
Halpern J. P., Mirabal N., 2006, GCN 5982
Hill G. et al., 2005, GCN 4255
Hjorth J. et al., 2003, Nat, 423, 847
Hogg D. W., Turner E. L., 1998, GCN 150
Holland S. et al., 2000, GCN 704
Hopkins A. M., Beacom J. F., 2006, ApJ, 615, 209
Infante L. et al., 2001, GCN 1152
Jakobsson P. et al., 2002, GCN 5782
Jakobsson P. et al., 2005, GCN 4017
Jakobsson P. et al., 2006a, GCN 5298
Jakobsson P. et al., 2006b, GCN 5320
Jakobsson P. et al., 2006c, GCN 5617
Jakobsson P. et al., 2006d, GCN 5698
Jakobsson P. et al., 2006e, A&A, 460, L13
Jakobsson P. et al., 2006f, GCN 5782
Jakobsson P. et al., 2007, GCN 6283
Jaunsen A. O. et al., 2007a, GCN 6010
Jaunsen A. O. et al., 2007b, GCN 6202
Jaunsen A. O. et al., 2007c, GCN 6216
Kann D. A. et al. 2007, ApJ, submitted (arXiv:0712.2186)
Kawai N. et al., 2005, GCN 3938
Kelson D. D., 2004, GCN 2627
Kelson D., Berger E., 2005, GCN 3101
Kistler M. D. et al., 2007, ApJ, 673, L119
Kouveliotou C. et al., 1993, ApJ, 413, L101
Kulkarni S. R. et al., 2002, GCN 1428
Le T., Dermer C. D., 2007, ApJ, 661, 394L
Le Floc'h E. et al., 2002, ApJ, 581, L81
Ledoux C. et al., 2006, GCN 5237
Levan A. J. et al., 2007, MNRAS, 378, 1439
Li L.-X., 2007, MNRAS, 388, 1487
Li L.-X., 2008, MNRAS, 388, 603
Liang E. W., Zhang B., 2006, ApJ, 638, L67
Liang E. W., Dai Z. G., 2004, ApJ, 606, L29
Liang E. W. et al., 2006, ApJ, 653, L81
Liang E. W., Zhang B., Virgili F., Dai Z. G., 2007, ApJ, 662, 1111
Lloyd-Ronning N. M., Fryer C., Ramirez-Ruiz E., 2002, ApJ, 574, 554
Lloyd-Ronning N. M., Dai X., Zhang B., 2004, ApJ, 601, 371
Maiorano E. et al., 2006, preprint (arXiv:astro-ph/0601293v1)
Martini P. et al., 2003, GCN 1980
Masseti N. et al., 2002, GCN 1330
Mazzali P. A. et al., 2006, Nat, 442, 1018
Mészáros P., 2006, Rep. Prog. Phys. 69, 2259
Mészáros P., 2007, ApJ, 655, L25
Mirabal N., Halpern J. P., 2006, GCN 4792
Mirabal N., Halpern J. P., An D. et al., 2006, ApJ, 643, L21
Nakar E., 2007, Physics Reports, 442, 166
Nardini M. et al., 2006, A&A, 451, 821
Norris J. P., 2002, ApJ, 579, 386
Norris J. P. et al., 2005, ApJ, 627, 324
Nysewander M., Fruchter A. S., Pe'er A. 2008, ApJ, submitted (arXiv:0806.3607)
Osip D. et al., 2006, GCN 5715
Paciesas W. S. et al., 1999, ApJS, 122, 465
Pian E. et al., 2006, Nat, 442, 1011
Piranomonte S. et al., 2006, GCN 4520
Porciani C., Madau P., 2001, ApJ, 548, 522
Preece R. D. et al., 2000, ApJS, 126, 19
Press W. H. et al., 1999, Numerical Recipes in Fortran. Cambridge Univ. Press, Cambridge
Price P. A., 2006b, GCN 5104
Price P. A. et al., 2002, GCN 1475
Price P. A. et al., 2003, GCN 1889
Price P. A. et al., 2004, GCN 2791
Price P. A. et al., 2006a, GCN 5275
Prochaska J. X. et al., 2003, GCN 2482
Prochaska J. X. et al., 2005a, GCN 3700
Prochaska J. X. et al., 2005b, GCN 3833
Prochaska J. X. et al., 2006, GCN 4593
Quimby R. et al., 2005, GCN 4221
Rol E. et al., 2003, GCN 1981
Rol E. et al., 2006, GCN 5555
Rowan-Robinson M., 1999, Ap&SS, 266, 291
Sakamoto T. et al., 2007, ApJ, 669, 1115
Schmidt M., 2001, ApJ, 552, 36
Schmidt M., 2004, ApJ, 616, 1072
Soderberg A. M. et al., 2002, GCN 1554
Soderberg A. M. et al., 2005, GCN 4186
Soderberg A. M. et al., 2006, Nat, 442, 1014
Soderberg A. M. et al., 2008, Nat, 453, 469
Stanek K. Z. et al., 2003, ApJ, 591, L17
Stern B. E. et al., 2001, ApJ, 563, 80
Stern B. E., Atteia J.-L., Hurley K., 2002, ApJ, 578, 304
Still M. et al., 2006, GCN 5226
Thoene C. C. et al., 2006, GCN 5812
Thoene C. C. et al., 2007a GCN, 6379
Thoene C. C. et al., 2007b, GCN 6499
Toma K., Ioka K., Sakamoto T., Nakamura T., 2007, ApJ, 659, 1420
Tinney C., 1998, International Astronomical Union Circulars 6896, 1
Vreeswijk P., Jaunsen A., 2006, GCN 4974
Vreeswijk P. et al., 2003a, GCN 1785
Vreeswijk P. et al., 2003b, GCN 1953
Vreeswijk P. et al., 2006, GCN 5535
Vreeswijk P. M. et al., 1999a, GCN 324
Vreeswijk P. M. et al., 1999b, GCN 496
Weidinger M. et al., 2003, GCN 2196
Wiersema K. et al., 2004, GCN 2800
Woosley S. E., 1993, ApJ, 405, 273
Xu, D., 2008, preprint (arXiv:0801.4325)
Zhang B., 2007, Chinese Journal of Astronomy & Astrophysics, 7, 1
Zhang B., Zhang B.-B., Liang E.-W. et al., 2007, ApJ, 655, L25
Zharikov S. V. et al., 1997, GCN3 31

This paper has been typeset from a TEX/LATEX file prepared by the author.